CSCanada
Energy Science and Technology
Vol. 2, No. 2, 2011, pp. 1-12
DOI:10.3968/j.est.1923847920110202.122

ISSN 1923-8460[PRINT]
ISSN 1923-8479[ONLINE]
www.cscanada.net
www.cscanada.org

Flow Distribution and Pressure Drop in Different Layout Configurations with Z-Type Arrangement

Junye Wang[1,*]

[1]Sustainable Soils and Grassland Systems Department, Rothamsted Research, North Wyke, Okehampton, Devon EX20 2SB, UK
[*]Corresponding author.
Email: junyewang@hotmail.com

Received 4 August 2011; accepted 8 November 2011

Abstracts

Bipolar plates (BPs) are a key component in fuel cells, which supply fuel and oxidant to reactive sites, remove water and heat, collect current and provide support for the cells in the stack. BPs typically account for 60~85% of the weight and 20~60% of the total cost in a fuel cell stack. It is well-known that performance of a fuel cell is stable in relatively narrow window operational conditions of electrochemistry. A small non-uniformity of flow distribution may lead significant deviation of some channels from the narrow window. Non-uniform flow distribution leads non-uniform electrochemical reactions and causes critical issues of flooding, drying and hotspots. Flow field designs in BPs are central to ensure uniform flow distribution and low pressure drop and to tackle systematically these critical issues. In spite of all the industrial R & D efforts, the gas flow fields in BPs remain one of the most important issues. In this paper, the generalised and unified theory developed by Wang (Int. J. of Hydrogen Energy 2010; 35: 5498-550) was extended to different layout configurations with Z-type arrangement in flow field designs of BPs. The present generalised theory has unique capacities to compare directly, systematically and quantitatively different configurations, existing models and methodologies. The theory makes a step forward in flow field designs in BPs, and provides practical guideline and measures to ensure uniform flow distribution in various configurations of BPs. This type of rational yet tractable generalised theory can contribute to the shared goal of cutting the currently high cost of R & D of fuel cells and performance improvement for commercialisation of fuel cells, which is central to a fuel cell engineer's "toolbox".

Key words: Bipolar plate; Fuel cell stack; Flow distribution; Manifold; Parallel channels; Pressure drop

Wang, J.Y. (2011). Flow Distribution and Pressure Drop in Different Layout Configurations with Z-Type Arrangement. *Energy Science and Technology*, *2*(2), 1-12. Available from: URL: http://www.cscanada.net/index.php/est/article/view/j.est.1923847920110202.122
DOI: http://dx.doi.org/10.3968/j.est.1923847920110202.122

Nomenclature

A	a coefficient in Eqs. (7) and (8), defined by Eq. (10)
B	constant in Eqs. (12), defined by Eq. (13)
C_t	coefficient of turning losses in channels
C_f	coefficients of turning losses in headers
d_h	hydraulic diameter of the channels (m)
D_h	hydraulic diameter of header (m)
E	Ratio of length to diameter
f	fanning friction factor
F	cross-sectional area of headers or channels (m^2)
F_m	surface area of porous materials (m^2)
H	Ratio of cross section areas (F_f/F_e)
J	constant in Eq. (12), defined by Eq. (14)
k	porous membrane permeability
l	length of the channels
L	length of header (m)
n	numbers of channels in a stack
m	number of turnings for serpentine flow fields
M	Ratio of sum of all the channel areas to intake header area ($F_c n/F_i$)
p	dimensionless pressure
P	pressure in header
Q	coefficient in Eq. (11), defined by Eq. (7)
Q_i	flow rate through porous materials
r	root of characteristic equation
R	coefficient in Eq. (11), defined by Eq. (8)

u dimensionless channel velocity
U channel velocity (m/s)
v_c dimensionless volume flow rate in the channels
w dimensionless velocity in header
W velocity in header (m/s)
x dimensionless axial coordinate in header
X axial coordinate in header (m) Greek symbols
β average velocity ratio in header (W_c/W)
ρ fluid density (kg/m^3)
τ wall shear stress (N/m^2)
ζ average total head loss coefficient for channel flow
ζ_m coefficient of membrane resistance
Subscripts
c channel
i intake header
e exhaust header

INTRODUCTION

Energy needs in the world continue to increase due to increase of population and the economic growth, driving demand at an unsustainable pace. Oil will not suddenly run out, but it is a finite resource. We must develop energy efficient technologies and renewable energy technologies that can stretch fossil fuel reserves while we modify our energy-use patterns and infrastructure to become more sustainable over the next few decades. A sustainable energy portfolio should include a variety of carbon-neutral technologies. Polymer electrolyte membrane (PEM) fuel cells are of greatest interests due to their clear advantages of low temperature, high power density, fast start-up and low emissions. A typical PEM fuel cell essentially consists of an anode backing, membrane electrode assembly (MEA) and cathode backing sandwiched between two bipolar plates (BPs). Fig. 1 presents a schematic of a highly parallelized fuel cell stack, as it can be conceived from a technical point of view. Each module (Fig. 2) comprises several layers that are stacked together and placed in housing with connectors. Each layer (Fig. 2) contains parallel channels of BPs. As the hydrogen and oxygen gases pass along the flow channels, they move into the gas diffusion layer (GDL) by diffusion and are consumed in the MEA causing the gas concentration to decrease along the flow channel.

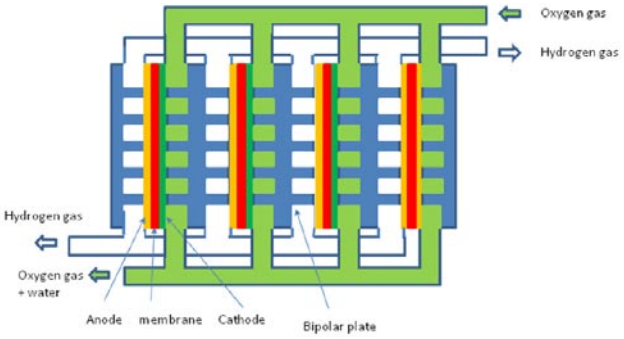

Figure 1
Schematic Diagram of Fuel Cell Stack and Bipolar Plates with Main Component

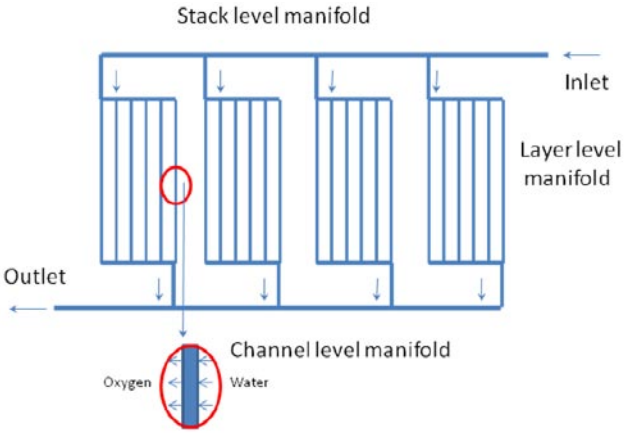

Figure 2
Schematic Diagram of Manifold Levels in a Fuel Cell Stack

The BPs, also known as the flow field plates, is one of the most important components which has numerous functions: 1) supplying fuel and oxidant for uniform distribution of them; 2) providing support for MEA; 3) separating gases between cells; 4) facilitating water and thermal management; and 5) conducting current. BPs typically account for 60~85% of the weight and 20~60% of the total cost influenced by the diverse range of factors, such as material, structure, manufacturing processes and technology in a fuel cell stack[1-5]. In spite of the variation, the BPs weight, volume and cost possess significant proportions of the overall stack. Therefore, there is a great potential to reduce significantly the weight, volume and cost of the fuel cell stack by optimising design of materials, flow field layout configuration, and fabrication techniques. However, the variety and complexity of flow fields in BPs, together with thermal and water management during dynamic operation process, have imposed a significant challenge on design and operation of BPs and PEM fuel cell stacks.

Water in the PEM fuel cells is an unavoidable product of the electrochemical reaction due to the presence of local oversaturated water vapour. Water is formed as a reaction product, and the amount of liquid and gaseous

water is determined by the concentration and temperature distribution inside the cell (and the relative humidity of the gases). During an operational cycle a fuel cell may go through the phases of flooding and drying. At high flow rates, the surface hydrophobicity of the diffusion media surface enhances efficacy of droplet removal, and may help to prevent local channel flooding. However, at low flow rates, hydrophobicity of the diffusion media surface has only a minimal impact on efficacy of droplet removal[6-9]. Barbir et al.[6] indicated that an increase in pressure drop, particularly on the cathode side of PEM fuel cell, is a reliable indicator of PEM fuel cell flooding, while an increase in cell resistance is a reliable indicator of fuel cell drying. Similarly, main causes of non-uniform heat and current density distribution are local variations in ohmic resistance and reactant rates, which come from local variations in reactant flow distributions[10-12]. Uneven heat and current production distribution can cause less efficient use of catalyst material and cell area. This can create dead zones where current production is significantly below the average or decrease cell life time, even component failure due to local hot spots and thermal stress concentration.

The goal of all the designs of flow field configurations is to ensure uniform reactant gas distributions, and low pressure drop over active electrode surface from the inlet to the outlet. At the same time, this will ensure product water removal and avoid membrane dehydration and hotspot. This means a high power density, durability and high efficiency. For a single channel design such as single serpentine, it is not difficult to find an optimal pressure and flow rates to avoid water flooding and drying and to maintain required water balance at inlet and outlet. However, the single serpentine design only has one long flow channel with a series of alternating 180° turns for the gas to flow through. A higher air compression pressure is required to push the gas through the long single channel which results in a high parasitic power loss. It is also possible that the high pressure may lead to dehydration of the membrane at the entrance of the field due to the high gas pressure and flooding near the channel exit due to the excessive liquid water carried downstream by the reactant gas stream. Moreover, this long channel may also result in a large decrease in reactant concentration from the inlet to the outlet causing fluctuation in current density across the MEA active area, resulting in a significant concentration gradient from the gas inlet to the outlet. Furthermore, a larger pressure gradient along the channel direction may result in considerable cross leakage flow between adjacent channels. This significant cross leakage flow through the porous electrode induces a strong convection in the electrode, bringing the reactant gas to the catalyst layer for electrochemical reaction and removing the product water from the reaction sites and electrodes. Therefore, for small fuel cells, single serpentine channels may be used where the pressure drop is of a smaller magnitude. However, for larger fuel cells, these styles of configurations will quickly increase the pressure drop to be of the order of a few bars due to the resistance increase of the flow turning losses and the channel length. Therefore, single serpentine layout is not the ideal flow field configuration due to the above problems.

It is well-known that performance of a PEM fuel cell is stable in relatively narrow window operational conditions, such as pressure, temperature, and flow rates. Thus, for a multiple channel configuration, such as straight parallel and multiple serpentine, flow distribution of reactants across channels plays a crucial role in the performance of the fuel cell and water and thermal management. A small non-uniformity of flow distribution may lead significant deviation of some channels from the narrow window. Thus, the performance of a channel may not be repeatable and reliable in other channels. When the flow rates and the pressure drop across channels are non-uniform, some individual channels allow the liquid water to accumulate to some extent due to low flow rate removal, and some allow membrane drying due to the high flow rates drying. The water accumulated in the cathode is usually removed out through GDL into the flow channels. As a result, the water accumulation in the channel or GDL leads gas flow resistance to rise, which in turn results in a further increase in the pressure drop between the inlet and outlet of the channel and causes uneven reaction rates, drying, water flooding, hotspot and fuel cell degradation. As a result, the system performance deteriorates totally the flow fields of the designs. Thus, the flow field designs are more obvious bottlenecks than chemistry, materials and manufacturing for commercialisation of fuel cells. Modelling and designs of flow field in BPs are a unique way to optimise systematically materials, layout configuration and fabrication techniques and has a great potential to reduce significantly weight, volume and cost of the fuel cell. Therefore, fuel cell stack design often boils down to bipolar plate design, which in turn is basically uniform flow distribution designs of the BPs.

In spite of all the industrial R & D efforts, there was the most important impediment to improving such models of flow distribution and pressure drop. In the past years, a broad spectrum of mathematical models and measurements has been proposed to provide timely information about how the cell performance will depend on key factors such as, layout and channel shape and size[13-16]. However, most of them did not include flow distribution in multiple channels. Few investigations have capacity to study relationships of configurations, structure and function in flow field designs due to complexity of manifold systems. The absence of such a synthesis makes it difficult to integrate the necessary disciplines for the design of key experiments. The process of increasing scientific understanding involves iteration between models and experiments, and in this sense models stimulate our thinking and inform our experiments. To predict how a

system will respond to change, it is necessary to quantify key processes, and the interactions between these key processes and the structure. Quantifying the complexity of flow and structure interactions in BPs or stacks can be difficult as system dynamics are often dependent on multi-physical and chemical processes. As our understanding progresses, a model should incorporate greater levels of realism, and more informative experiments can be designed as applying the models will show what we need to measure and how it should be measured. Thus, applying models will also help us to address questions of scale and identify how configurations and structures function. Therefore, flow field designs in BPs are now at the exciting stage of beginning to formulate a synthesis for stimulating the scientific debate.

Wang[17-18] did the first attempt to unify main theoretical models into one theoretical framework for parallel channel configurations. The main existing models and solution methods were unified to one theoretical framework for parallel channel configuration, including Bernoulli theory and momentum theory, and discrete and continuum methodologies. Then, his model has been extended to describe other configurations with U type arrangement, including single serpentine, multiple serpentine, parallel straight channel, interdigitated and pin-type configurations[19]. Bernoulli equation is a special case of the present flow models in manifolds. It is also obvious that the existing model by Bajura[20-21] and by Bassiouny and Martin[22] is a special case of the present solutions without the friction effect and those by Kee et al.[23] and Maharudrayya et al.[24] are another special case without inertial effect. More models[25-27] can be included in this theoretical framework using simple modification of coefficients. Therefore, the present model includes almost all the main existing models. In this regard, a fruitfully unified perspective is now emerging—one quite natural to fuel cell engineers.

In this paper, we will extend the generalised theoretical models of Z-type arrangement developed by Wang[18] from the parallel straight channels to other most common layout configurations with Z-type arrangement, including single serpentine, multiple serpentine, and interdigitated layouts using the physical parameters of the structures: ratio of length to diameter and ratio of all the channel areas to head area for determining the performances of different layout configurations. Then, a direct, systematic and quantitative comparison of performances will be carried out among the most common layout configurations. This establishes organic and quantitative linkage of performances between different layout configurations for the robust layout designs and provides a practical guadeline how to determine channel number, channel shape and layout for a given active area, channel shape and operating conditions. This will provide practical measures to tackle systematically critical issue of water, thermal and current management through uniform flow distribution design in an easy and cheap approach.

1. THEORY OF FLOW FIELD DESIGNS

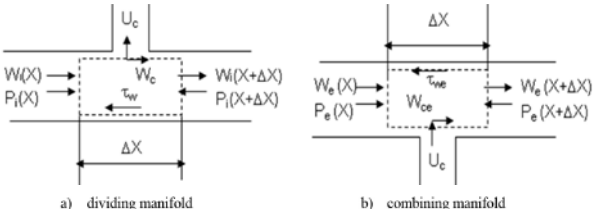

Figure 3
Control Volumes in Manifolds: a) Dividing Manifold, and b)Combining Manifold

Flow field designs in bipolar plates are to distribute uniformly fluids in active areas to maintain uniform electrochemical rates, which is essentially a strategy of flow distribution in manifold systems. Uniform electrochemical reactions can ensure a high performance and long life time. Manifold systems are usually employed in fuel cells, which are categorised into one of the two possible combinations of dividing and combining flow manifolds: U-arrangement and Z-arrangement. It should be mentioned that the model in Ref.[18] was used for the straight parallel configurations. Here we modify it for use of other most common configurations with Z-type arrangement and any shapes. Following the derivation in Ref.[18], mass and momentum balances can be written based on the control volumes in dividing and combining manifolds (Fig. 3) as follows:

$$\frac{dw_i}{dx}\frac{d^2w_i}{dx^2}+\left\{\frac{(2-\beta_i)}{\zeta}\left(\frac{F_c n}{F_i}\right)^2-\left(1-\frac{f_i D_{hi}}{\upsilon(\mathrm{Re}_i f_i)}\right)\frac{2-\beta_e}{\zeta}\left(\frac{F_c n}{F_e}\right)^2\right\}w_i\frac{dw_i}{dx}$$
$$+\left\{\frac{L}{2\zeta}\frac{f_i}{D_{hi}}\left(\frac{F_c n}{F_i}\right)^2-\left(1-\frac{2f_i D_{hi}}{\upsilon(\mathrm{Re}_i f_i)}\right)\frac{f_e L}{2\zeta D_{he}}\left(\frac{F_c n}{F_e}\right)^2\right\}w_i^2=\frac{f_e L}{2\zeta D_{he}}\left(\frac{F_c n}{F_e}\right)^2 \quad (1)$$

where F_i, F_e and F_c are the cross-sectional areas of the intake header, exhaust header and the channel (m^2), respectively, F_i, F_e and F_c the frictional coefficients of the intake header, the exhaust header and the channel, respectively, β_i and β_e the average velocity ratio in header of the intake header and the exhaust header, respectively, D_{hi} and D_{he} the hydraulic diameter of intake header and exhaust header (m), respectively, w_i the normalised axial velocity in intake header, n is the number of channels, ζ average total head loss coefficient for channel flow, L length of the header, and x normalised axial coordinate in the header.

$$p_i - p_e = \frac{1}{2}\zeta\left(\frac{F_i}{F_c n}\right)^2\left(\frac{dw_i}{dx}\right)^2 \quad (2)$$

Where p_i and p_e are pressure of intake and exhaust header respectively, and

$$\zeta = 1 + C_{fi} + mC_t + C_{fe} + f\frac{l}{d_h} \tag{3}$$

where C_{fi} is coefficient of turning loss from the intake header into the channels, mC_t is product of number of m turns and turning loss, C_t, for serpentine configurations, C_{fe} that of turning losses from the channels into the exhaust header, and f is average friction coefficient for the channel flow, d_h and l are hydraulic diameter and length of channels respectively. It can be seen that Eq. (1) can be simplified to that of Bernoulli equation when β_i and β_e are equal to one.

For interdigitated type, we define that the pressure drop between p_i and p_e are sum of average total head loss for the channel flow and head loss of porous media. Thus the coefficient of the total head loss can be described as follows:

$$\zeta=\zeta_1+\zeta_{mem} \tag{4}$$

where

$$\zeta_1 = 1 + C_{fi} + mC_t + C_{fe} + f\frac{l}{d_h} \tag{5}$$

where ζ_{mem} is the membrane resistance through porous materials.

The most common phenomenological description of flow through porous materials is Darcy's law:

$$Q_i = \frac{\Delta P}{F_m \zeta_{mem}} \tag{6}$$

Where Q_i is flow rate through porous membrane and F_m is surface area of porous materials. We assume that the membrane resistance, ζ_{mem} is simply the inverse of the membrane permeability, k ($\zeta_{mem}=a/k$).

Eqs. (1) and (4) use hydraulic diameters to replace practical one which are different from those in Ref.[18]. Thus, the model can be used for any shapes[28]. It should be noted that Eq. (3) different from Eq. (11) in Ref.[18] has a term which describes turning losses in channels. Eq. (1) was solved analytically by Wang[18] for the first time for the straight parallel configurations in 2010. Hereinafter the model will be used for single serpentine, multiple serpentine, straight parallel, and interdigitated flow field layout configurations since all the layouts can be simplified into a manifold system with two manifolds for dividing and combing fluids.

There were numerous numerical solutions of Eq. (1) in past fifty years[25-29]. The numerical work required an iterative numerical procedure which was quite cumbersome. It may be long and tedious when there are many channels for design purposes. Furthermore, they had to use graphs or tables to present relationship between geometries and flow conditions. This was incomplete due to the variety and complexity of geometrical structure. Because of no direct relation between flow performance and geometries, the numerical solution would have to be used in a trial- and -error fashion. Particularly it was also inconvenient for a designer to use it in preliminary design in which we have less information if a geometrical structure is optimal but major decisions should be made in this stage. A mathematical models is, in fact, needed to provide timely information about how to interact between performance and structure. An analytical solution, in this regard, will play an important role in cutting the currently high cost and long time for R & D of PEM fuel cells. For the sake of self-contained papers and for later use the analytical solutions by Wang[18] are reproduced partly for Z-type here.

2. ANALYTICAL SOLUTION

To use, we redefine three constants using the practical parameters of the structure:

$$\begin{aligned} Q &= \frac{(2-\beta_i)}{3\zeta}\left(\frac{F_c n}{F_i}\right)^2 - \left(1-\frac{f_i D_i}{\upsilon(\mathrm{Re}_i f_i)}\right)\frac{2-\beta_e}{3\zeta}\left(\frac{F_c n}{F_e}\right)^2 \\ &= \frac{(2-\beta_i)}{3\zeta}\left(\frac{F_c n}{F_i}\right)^2\left[1-\left(1-\frac{f_i D_i}{\upsilon(\mathrm{Re}_i f_i)}\right)\frac{2-\beta_e}{2-\beta_i}\left(\frac{F_i}{F_e}\right)^2\right] \\ &= \frac{(2-\beta_i)}{3\zeta}M^2\left[1-(1-A)\frac{(2-\beta_e)}{(2-\beta_i)}H^2\right] \end{aligned} \tag{7}$$

$$\begin{aligned} R &= -\frac{L}{4\zeta}\frac{f_i}{D_i}\left(\frac{F_c n}{F_i}\right)^2 + \left(1-\frac{2f_i D_i}{\upsilon(\mathrm{Re}_i f_i)}\right)\frac{f_e L}{4\zeta D_e}\left(\frac{F_c n}{F_e}\right)^2 \\ &= -\frac{L}{4\zeta}\left[\frac{f_i}{D_i}-\frac{f_e}{D_e}\left(1-\frac{2f_i D_i}{\upsilon(\mathrm{Re}_i f_i)}\right)\left(\frac{F_i}{F_e}\right)^2\right]\left(\frac{F_c n}{F_e}\right)^2 \\ &= -\frac{E}{4\zeta}\left[\frac{f_i}{D_i}-\frac{f_e}{D_e}(1-2A)H^2\right]M^2 \end{aligned} \tag{8}$$

$$\varepsilon = -\frac{f_e L}{2\zeta D_e}\left(\frac{F_c n}{F_e}\right)^2 = -\frac{E f_e}{2\zeta}M^2 \tag{9}$$

For sake of simplicity, we assume $D_i=D_e=D_h$
where

$$M = \frac{F_c n}{F_i},\ E = \frac{L}{D_h},\ H = \frac{F_i}{F_e} \text{ and } A = \frac{f_i D_i}{\upsilon(\mathrm{Re}_i f_i)} \tag{10}$$

Thus, Eq. (21) is reduced as follows:

$$\frac{dw_i}{dx}\frac{d^2 w_i}{dx^2} + 3Qw_i\frac{dw_i}{dx} - 2Rw_i^2 = -\varepsilon \tag{11}$$

Its general solution of the homogeneous version of Eq. (11) as follows:

$$\begin{cases} r = B \\ r_1 = -\frac{1}{2}B + \frac{1}{2}i\sqrt{3}J \\ r_2 = -\frac{1}{2}B - \frac{1}{2}i\sqrt{3}J \end{cases} \tag{12}$$

Where

$$B = \left[R + \sqrt{Q^3 + R^2}\right]^{1/3} + \left[R - \sqrt{Q^3 + R^2}\right]^{1/3} \tag{13}$$

$$J = \left[R + \sqrt{Q^3 + R^2}\right]^{1/3} - \left[R - \sqrt{Q^3 + R^2}\right]^{1/3} \tag{14}$$

Let's assuming a particular solution to Eq. (11), $w^* = \sqrt{k}$. Thus, its first and second derivatives are as follows:

$w^{*'}=0$

$w^{*''}=0$

Inserting the particular solution and its derivatives into Eq. (11), we have:

$-2Rk=-\varepsilon$

$k=\varepsilon/2R$

$$w^* = \sqrt{\varepsilon/2R} \tag{15}$$

Similar to the analysis in Ref.[18], determining which roots of Eq. (12) are real and which are complex can be accomplished by noting that if the polynomial discriminant $Q^3+R^2>0$, one root is real and two are complex conjugates; if $Q^3+R^2=0$, all roots are real and at least two are equal; and if $Q^3+R^2<0$, all roots are real and unequal.

Thus, we have two sets of solutions of Eq. (12). One solution is $r=B$ which represents a case of no fluid flow in BPs or the stack. Another set is two conjugated solutions, r_1 and r_2. Let's take the two conjugated solutions into account which will depend on the sign of R^2+Q^3.

Case 1: $R^2+Q^3<0$

Defining $\theta = \cos^{-1}\left(\frac{R}{\sqrt{-Q^3}}\right)$, and substituting it into Eq. (12), Eq. (12) can be reduced to:

$$r_1 = 2\sqrt{-Q}\cos\left(\frac{\theta}{3}\right)$$

$$r_2 = 2\sqrt{-Q}\cos\left(\frac{\theta + 2\pi}{3}\right)$$

Thus, the general solution of Eq. (11) and boundary conditions can be written as follows:

$$\begin{aligned} &w_i = C_1 e^{r_1 x} + C_2 e^{r_2 x} + \sqrt{\varepsilon/2R} \\ &w_i = 0, \quad at\, x = 1 \\ &w_i = 1, \quad at\, x = 0 \end{aligned} \tag{16}$$

Axial velocity in the intake and exhaust manifolds:

$$w_i = \frac{\left(e^{r_1+r_2 x} - e^{r_2+r_1 x}\right)}{e^{r_1} - e^{r_2}} + \sqrt{\frac{\varepsilon}{2R}}\left[1 - \frac{e^{r_1+r_2 x} - e^{r_2+r_1 x}}{e^{r_1} - e^{r_2}} - \frac{e^{r_1 x} - e^{r_2 x}}{e^{r_1} - e^{r_2}}\right] \tag{17}$$

$$w_e = \left[1 - \frac{\left(1 - \sqrt{\frac{\varepsilon}{2R}}\right)\left(e^{r_1+r_2 x} - e^{r_2+r_1 x}\right)}{e^{r_1} - e^{r_2}} - \frac{\sqrt{\frac{\varepsilon}{2R}}\left(e^{r_1 x} - e^{r_2 x}\right)}{e^{r_1} - e^{r_2}} + \sqrt{\frac{\varepsilon}{2R}}\right]\frac{F_i}{F_e} \tag{18}$$

Channel velocity:

$$u_c = -\frac{F_i}{F_c n}\frac{dw_i}{dx} = -\frac{F_i}{F_c n}\left\{\frac{\left(1 - \sqrt{\frac{\varepsilon}{2R}}\right)\left(r_2 e^{r_1+r_2 x} - r_1 e^{r_2+r_1 x}\right)}{e^{r_1} - e^{r_2}} - \frac{\sqrt{\frac{\varepsilon}{2R}}\left(r_1 e^{r_1 x} - r_2 e^{r_2 x}\right)}{e^{r_1} - e^{r_2}}\right\} \tag{19}$$

Flow distribution:

$$v_c = -\frac{r_2 e^{r_1+r_2 x} - r_1 e^{r_2+r_1 x}}{e^{r_1} - e^{r_2}} + \sqrt{\frac{\varepsilon}{2R}}\frac{1}{e^{r_1} - e^{r_2}}\left[\left(r_2 e^{r_1+r_2 x} - r_1 e^{r_2+r_1 x}\right) + \left(r_1 e^{r_1 x} - r_2 e^{r_2 x}\right)\right] \tag{20}$$

Pressure drop in the channels:

$$p_i - p_e = \frac{1}{2}\zeta\left(\frac{F_i}{F_c n}\right)^2\left\{\frac{\left(1 - \sqrt{\frac{\varepsilon}{2R}}\right)\left(r_2 e^{r_1+r_2 x} - r_1 e^{r_2+r_1 x}\right)}{e^{r_1} - e^{r_2}} - \frac{\sqrt{\frac{\varepsilon}{2R}}\left(r_1 e^{r_1 x} - r_2 e^{r_2 x}\right)}{e^{r_1} - e^{r_2}}\right\}^2 \tag{21}$$

Case 2: $R^2+Q^3=0$

Two conjugated solutions of the characteristic equation can be reduced as follows:

$$r_1 = r_2 = -\frac{1}{2}R^{1/3} = r$$

Thus, the general solution of Eq. (11) and its boundary conditions can be written as follows:

$$\begin{aligned} &w_i = \left(C_1 + C_2 x\right)e^{rx} + \sqrt{\varepsilon/2R} \\ &w_i = 0, \quad at\, x = 1 \\ &w_i = 1, \quad at\, x = 0 \end{aligned} \tag{22}$$

Axial velocity in the intake and exhaust header:

$$w_i = (1-x)e^{rx} + \sqrt{\frac{\varepsilon}{2R}}\left(1 - e^{rx} + xe^{rx} - xe^{r(x-1)}\right) \tag{23}$$

$$w_e = \left\{1 - \left[(1-x)e^{rx} + \sqrt{\frac{\varepsilon}{2R}}\left(1 - e^{rx} + xe^{rx} - xe^{r(x-1)}\right)\right]\right\}\frac{F_i}{F_e} \tag{24}$$

Channel velocity:

$$u_c = -\frac{F_i}{F_c n}\frac{dw_i}{dx} = -\frac{F_i}{F_c n}\left\{\left(1 - \sqrt{\frac{\varepsilon}{2R}}\right)re^{rx} - (1+rx)\left(1 - \sqrt{\frac{\varepsilon}{2R}} + \sqrt{\frac{\varepsilon}{2R}}\frac{1}{e^r}\right)e^{rx}\right\} \tag{25}$$

Flow distribution:

$$\begin{aligned} v_c &= \frac{F_c U_c}{F_i W_0/n} = \frac{nF_c}{F_i}u_c \\ &= (1 - r + rx)e^{rx} - \sqrt{\frac{\varepsilon}{2R}}\left[(1 - r + rx)e^{rx} - (1+rx)e^{r(x-1)}\right] \end{aligned} \tag{26}$$

Pressure drop in the channels:

$$p_i - p_e = \frac{1}{2}\zeta\left(\frac{F_i}{F_c n}\right)^2\left\{\left(1 - \sqrt{\frac{\varepsilon}{2R}}\right)re^{rx} - (1+rx)\left(1 - \sqrt{\frac{\varepsilon}{2R}} + \sqrt{\frac{\varepsilon}{2R}}\frac{1}{e^r}\right)e^{rx}\right\}^2 \tag{27}$$

Case 3: $R^2+Q^3>0$

Two conjugated solutions retain same as Eq. (12):

$$r_1 = -\frac{1}{2}B + \frac{1}{2}i\sqrt{3}J$$

$$r_2 = -\frac{1}{2}B - \frac{1}{2}i\sqrt{3}J$$

Thus, the general solution of Eq. (11) and boundary conditions can be written as follows:

$$\begin{aligned} w_i &= e^{-Bx/2}\left[C_1\cos\left(\sqrt{3}Jx/2\right) + C_2\sin\left(\sqrt{3}Jx/2\right)\right] + \sqrt{\varepsilon/2R} \\ w_i &= 0, \quad at\, x = 1 \\ w_i &= 1, \quad at\, x = 0 \end{aligned} \tag{28}$$

Axial velocity in the intake and exhaust header:

$$w_i = \frac{\sin\left(\frac{\sqrt{3}}{2}J(1-x)\right)}{\sin\left(\frac{\sqrt{3}}{2}J\right)}e^{-Bx/2} + \sqrt{\frac{\varepsilon}{2R}}\left\{1 - \frac{\sin\left(\frac{\sqrt{3}}{2}Jx\right)}{\sin\left(\frac{\sqrt{3}}{2}J\right)}e^{B(1-x)/2} - \frac{\sin\left(\frac{\sqrt{3}}{2}J(1-x)\right)}{\sin\left(\frac{\sqrt{3}}{2}J\right)}e^{-Bx/2}\right\} \tag{29}$$

$$w_e = \left\{1 - \frac{e^{-Bx/2}}{\sin\left(\frac{\sqrt{3}}{2}J\right)}\left[-\sqrt{\frac{\varepsilon}{2R}}e^{B/2}\sin\left(\frac{\sqrt{3}}{2}Jx\right) + \left(1 - \sqrt{\frac{\varepsilon}{2R}}\right)\sin\left(\frac{\sqrt{3}}{2}J(1-x)\right)\right] - \sqrt{\frac{\varepsilon}{2R}}\right\}\frac{F_i}{F_e} \tag{30}$$

Channel velocity:

$$u_c = -\frac{F_i}{F_c n}\frac{dw_i}{dx} =$$

$$-\frac{e^{-Bx/2}}{\sin\left(\frac{\sqrt{3}}{2}J\right)}\frac{F_i}{F_c n}\left\{\begin{aligned}&\frac{B}{2}\sqrt{\frac{\varepsilon}{2R}}e^{B/2}\sin\left(\frac{\sqrt{3}}{2}Jx\right) - \frac{B}{2}\left(1 - \sqrt{\frac{\varepsilon}{2R}}\right)\sin\left(\frac{\sqrt{3}}{2}J(1-x)\right) \\ &-\sqrt{\frac{\varepsilon}{2R}}e^{B/2}\frac{\sqrt{3}}{2}J\cos\left(\frac{\sqrt{3}}{2}Jx\right) - \left(1 - \sqrt{\frac{\varepsilon}{2R}}\right)\frac{\sqrt{3}}{2}J\cos\left(\frac{\sqrt{3}}{2}J(1-x)\right)\end{aligned}\right\} \tag{31}$$

Flow distribution:

$$v_c = \frac{e^{-Bx/2}}{2\sin\left(\frac{\sqrt{3}}{2}J\right)}\left[B\sin\left(\frac{\sqrt{3}}{2}J(1-x)\right) + \sqrt{3}J\cos\left(\frac{\sqrt{3}}{2}J(1-x)\right)\right] - \frac{e^{-Bx/2}}{2\sin\left(\frac{\sqrt{3}}{2}J\right)}\sqrt{\frac{\varepsilon}{2R}}$$

$$\left\{\left[B\sin\left(\frac{\sqrt{3}}{2}J(1-x)\right) + \sqrt{3}J\cos\left(\frac{\sqrt{3}}{2}J(1-x)\right)\right] + e^{B/2}\left[B\sin\left(\frac{\sqrt{3}}{2}Jx\right) - \sqrt{3}J\cos\left(\frac{\sqrt{3}}{2}Jx\right)\right]\right\} \tag{32}$$

Pressure drop in the channels:

$$p_i - p_e = \frac{1}{2}\zeta\left(\frac{F_i}{F_c n}\right)^2\left(\frac{dw_i}{dx}\right)^2$$

$$= \frac{1}{2}\zeta\left(\frac{F_i}{F_c n}\right)^2\frac{e^{-Bx}}{\sin^2\left(\frac{\sqrt{3}}{2}J\right)}\left\{\begin{aligned}&\frac{B}{2}\sqrt{\frac{\varepsilon}{2R}}e^{B/2}\sin\left(\frac{\sqrt{3}}{2}Jx\right) - \frac{B}{2}\left(1 - \sqrt{\frac{\varepsilon}{2R}}\right)\sin\left(\frac{\sqrt{3}}{2}J(1-x)\right) \\ &-\sqrt{\frac{\varepsilon}{2R}}e^{B/2}\frac{\sqrt{3}}{2}J\cos\left(\frac{\sqrt{3}}{2}Jx\right) - \left(1 - \sqrt{\frac{\varepsilon}{2R}}\right)\frac{\sqrt{3}}{2}J\cos\left(\frac{\sqrt{3}}{2}J(1-x)\right)\end{aligned}\right\}^2 \tag{33}$$

3. ANALYSIS OF FLOW FIELD LAYOUT DESIGNS WITH Z-TYPE ARRANGEMENT

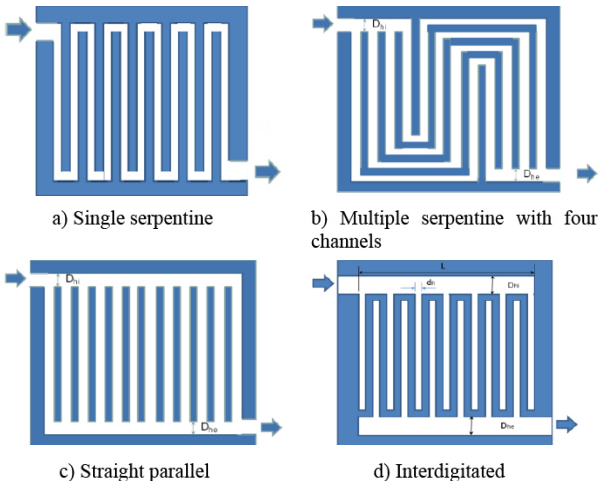

a) Single serpentine b) Multiple serpentine with four channels c) Straight parallel d) Interdigitated

Figure 4
Layout Configurations of Bipolar Plates: a) Single Serpentine, b) Multiple Serpentine with Four Channels, c) Straight Parallel and d) Interdigitated

To compare flow field designs of the different layouts, we used the same shapes and dimensions of channels under the same active area as shown in Fig. 4. Thus, there is a certain relationship between the channel number and channel length for single serpentine, multiple serpentine, straight parallel and interdigitated configurations. As a limited case, the straight parallel configuration has the most channel number and the shortest length of the channels. Another limited case is the single serpentine configurations which has the longest unique channel. Corresponding E (L/D), M (nF_c/F_i) and ζ can be calculated directly after a given active area and manifold with approximate proportions for different configurations. For sake of simplicity, we list E (L/D), M (nF_c/F_i) and ζ in Table 1 according to approximate proportions for different configurations in Fig. 4. Therefore, it is possible to have a quantitative comparison between different configurations, particularly between the straight parallel channel and the multiple serpentine configurations using the present analytical solutions.

Table 1
Relationship of Channel Number and Two Ratios in Different Layout Configurations for the Same Active Area and Channel Dimensions

Layout configurations	Channel Number	E (L/D)	ζ	M (nF_c/F_i)
single serpentine in Fig. 4a	1	0.5	14	0.5
multiple serpentine with four channels in Fig. 4b	4	3.5	4.5	2
Straight parallel in Fig. 4d	12	12	1	6
Interdigitated in Fig. 4e	12	12	40	6

3.1 Axial Velocity in the Intake Manifold

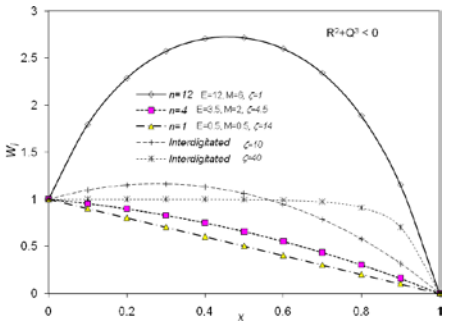

a) $R^2+Q^3<0$

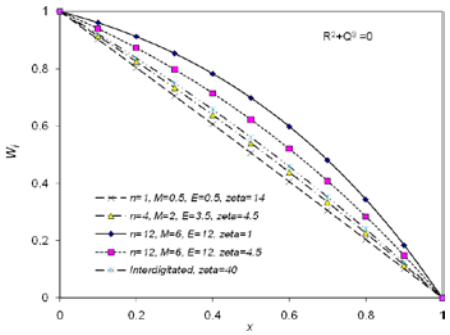

b) $R^2+Q^3=0$

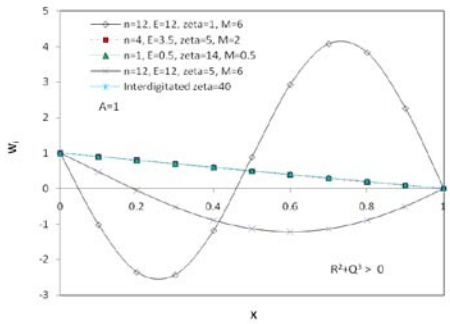

c) $R^2+Q^3>0$

Figure 5
Axial Velocity Profiles of Different Configurations: a) $R^2+Q^3<0$, b) $R^2+Q^3=0$ and c) $R^2+Q^3>0$.

Fig. 5 shows comparisons of axial velocity profiles between different configurations. It can be seen that the axial velocities decrease along intake header for the single serpentine configuration. They are linearly falling with x-axis. The nonlinearity increases as the channel number increases. There is the largest nonlinearity for the straight parallel configurations for all the three flow regions. However, there is an obvious difference between three flow regions. The axial velocities increase first and then turn into decrease steeply for the straight parallel configuration for $R^2+Q^3<0$ (Fig. 4a) while the axial velocities oscillate along x-axis for $R^2+Q^3>0$ (Fig. 5c). The velocity profiles are different from those in U-type arrangement for the straight parallel configuration[27]. U-type arrangements generally present a better profile.

For $R^2+Q^3=0$, the two roots of the characteristic equation were reduced to $r_1 = r_2 = -\frac{1}{2}R^{1/3} = r$ in which the solutions of Eq. (1) are only dependent on R. Hence, there is no influence of Q on the axial velocity distribution. It can be easily seen that the axial velocities in all the configurations decrease along axis. The increase of the channel number in the multiple serpentine does increase nonlinearity. However, the axial velocity profiles are much better than those at $R^2+Q^3<0$ and $R^2+Q^3>0$, particularly for the straight parallel configurations. In practice, the values of R and Q are determined by geometries and flow coefficients. In a practical design, it is not easy to keep that R^2+Q^3 is exactly equal to 0. Here the showcases are nearly equal to 0. However, the case can give an insight of all the flow regions and a practical measure to improve flow distributions.

In addition, it can be seen that the interdigitated type can have better axial velocity profiles than the straight parallel dur to a big resistance of the channels. Here the ζ represents the resistance of the channels in the model. Due to the fact that the most of the pressure drop occurs in the porous media, the uniformity of flow distribution between individual channels strongly depends on uniformity of GDL thickness and effective porosity permeability for the interdigitated configurations. Therefore, both flow distribution and pressure drop of this flow field are mainly determined by the properties of the porous media through the parameter ζ in the model.

3.2 Flow Distribution

Fig. 6 shows the influence of the layout configurations on flow distribution in the channels. The single serpentine has the best flow distribution (it is always uniform as expected) (Fig. 4a). The straight parallel configuration has the worst flow distribution. The multiple serpentine is between the straight parallel and the single serpentine configurations.

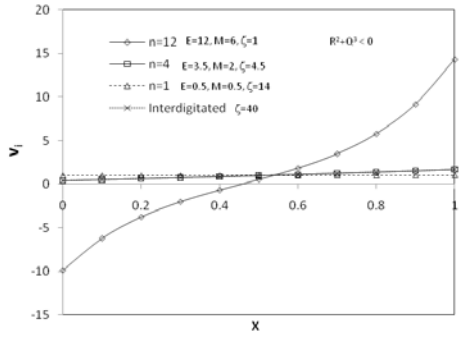

a) $R^2+Q^3<0$

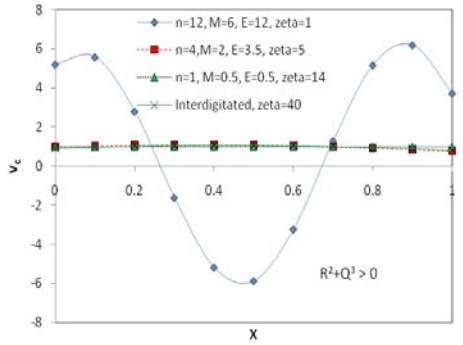

b) $R^2+Q^3>0$

Figure 6
Flow Distributions in Different Configurations: a) $R^2+Q^3<0$, and b) $R^2+Q^3>0$

Multiple serpentine flow field designs are between straight parallel-channels and single serpentine in mind. These consist of multiple shorter serpentine channels connected at inlet and outlet manifolds as shown in Fig. 4b. This style of flow fields is variations of a single serpentine pattern or a straight parallel pattern. Therefore, this type has the same features of the single channel serpentine except a lower pressure drop. On the other hand, it has the same feature as the straight parallel since parallel channels have been employed. Thus, uniform flow distribution is also a critical issue of this type design.

The straight parallel configurations (Fig. 4c), are typically used when no accumulation of water droplets is expected. The configurations of the straight parallel-channel possess a clear advantage of simplicity and the lowest pressure drop over all the serpentine and interdigitated styles which mean the smallest parasite losses and the lowest fabricated cost. However, using the configurations of the straight parallel-channel does have possibility of the severe flow mal-distribution problems, which reduces fuel cell performance. If droplets form, they may block one or more of the parallel channels, while the remaining gas stream flows through the least blocked channels. However, the non-uniformity of flow distribution in both the straight parallel and the multiple serpentine configurations are not inherent rather than a poor design. There are three characteristic parameters which can be adjusted to improve the flow distribution and pressure drop of flow fields of BPs, namely, the ratio of total loss coefficient of channels ζ, ratio of header length to header diameter E (L/D), and ratio of sum of the areas of all channels to the cross-sectional area of header M (nF_c/F_i). An appreciate selection of these parameters do improve greatly uniformity of flow distribution[27]. This implys an possibility of optimal designs.

3.3 Pressure Drops of Different Layout Configurations

Fig. 7 shows pressure drops of different layout configurations. Pressure drops were affected greatly by the layout configurations. The straight parallel configuration has the lowest pressure drops. The single serpentine has the highest pressure drops which is as about 100 times as those of the straight parallel configurations in the present cases. It can be seen that the pressure drops in the multiple serpentine decrease significantly with increasing the channel number. The single serpentine design has one long flow channel with a series of alternating 180° turns for the gas to flow through. Along the single serpentine, oxygen depletes with the length of path (Fig. 4a), leading to a decrease in current density along the channel. It is the primary benefit provided by the single channel design is that flow distribution is always uniform. This ensures that any water formed is removed under a higher pressure drop. However, a long channel means a high flow resistance, and a higher air compression pressures are required to push the gas through the long single channel which results in high parasitic power losses. It is also possible that the high pressure may lead to dehydration of the membrane at the entrance of the field due to high gas pressure and flooding near the channel exit due to excessive liquid water carried downstream by the reactant gas stream. Moreover, this long channel may also result in a large decrease in reactant concentration from inlet to outlet causing fluctuation in current density across the MEA active area, resulting in a significant concentration gradient from gas inlet to outlet. Furthermore, a larger pressure gradient along the channel direction may result in considerable cross leakage flow between the adjacent channels. This significant cross leakage flow through the porous electrode induces a strong convection in the electrode, bringing the reactant gas to the catalyst layer for electrochemical reaction and removing the product water from the reaction sites and electrodes.

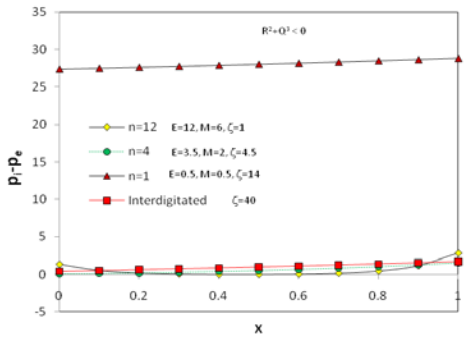

a) $R^2+Q^3<0$

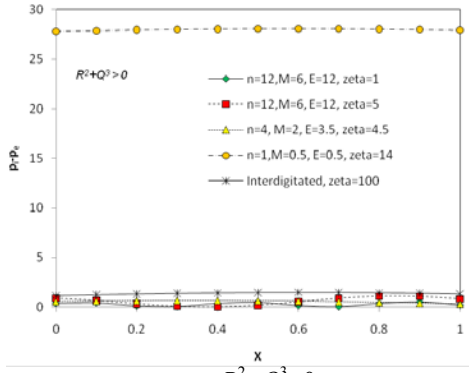

b) $R^2+Q^3>0$

Figure 7
Pressure Drops of Different Layout Configurations: a) $R^2+Q^3<0$, and b) $R^2+Q^3>0$

The pressure drop in a multiple serpentine is between the straight parallel and the single serpentine configurations. This is in agreement with those of U-type arrangements[27]. PEM fuel cells with serpentine flow channels tend to have the best performance and durability/ reliability. Because of uniform reactant distribution, the polymer membrane can remain hydrated to maintain its protonic conductivity, and water produced by the reaction can be removed from the cathode only when pressure drop is between the two thresholds. The present results showed that a compromise between pressure drop and flow distribution can be achieved easily by balance between channel length and channel number. Thus, the serpentine flow channel layout is the most widely known and used under the same operating and design conditions.

The results indicate that the single serpentine design is obviously not an ideal design and leads a substantial pressure drop (large paraside power losses). So-called optimal designs are therefore related to multiple serpentine and straight parallel configurations. All these results demonstrate possibility of the optimal design for the fuel cell configurations. Particularly, it is possible to improve greatly flow uniformity of the straight parallel and the multple serpentine configurations. Non-uniform of flow distribution in a straight parallel configuration is not inherent rather than as a result of poor design. Furthermore, the straight parallel configurations possess simpler structures. This implys easy manufacturing and low cost. Thus, we have much more practical measures to achieve low pressure drop and uniform flow distribution, namely, a high performance and low cost.

4. DISCUSSIONS

Although it is well-known that the main design philosophy is based on the determination of an appropriate pressure drop and uniform flow distribution along and across the flow channels so that all the channels in the cell have the same pressure drop and flow rates, no systematic and quantitative relationships were established between flow distribution, configuration and structures and main existing models may suffer a significant error[30]. We knew that the critical issues of water flooding and drying and hotspots are due to non-uniform flow distributions[1-5]. And the single serpentine has high pressure drop but we did not know how much high it compared to the straight parallel. We also knew that the straight parallel may experience severe problems of non-uniform flow distribution but we did not know how much the non-uniformity can be improved. Thus, the knowledge of a channel can not be upscaled to all the parallel channels. Active approaches have to be employed to mitigate the water and heat management issues. Many of the strategic methods used to water and thermal managements lead to increased system volume and complexity, such as the use of extra systems or components (external valves, cooling or pumps). Furthermore, modifying the operating conditions in fuel cell systems is one of common strategies of water and heat mitigation, which may deviate from optimal design conditions.

In all the cases, the layout configurations do affect significantly flow distribution and the pressure drop. This demostrates theoretically that the flow field designs are more obvious bottlenecks than chemistry, materials and manufacturing for the commercialisation of fuel cells. For the same active area, the multiple serpentine type is between the straight parallel and the single serpentine configurations. The straight parallel configuration has the most possibility with uneven flow distribution across the channels. The single serpentine has the best flow distribution (it is always uniform). However, the straight parallel configuration has the smallest pressure drops. The single serpentine has the largest pressure drops. The pressure drop in a multiple serpentine is between the straight parallel and the single serpentine configurations. The pressure drop in the single serpentine may be as a hundred times as those in the straight parallel configurations.

The results show that the non-uniformity of flow distribution in both the straight parallel and the multiple serpentine configurations are not inherent rather than a poor design. Three characteristic parameters (the ratio of total loss coefficient of channels ζ, ratio of header length

to header diameter E (L/D), and ratio of sum of the areas of all channels to the cross-sectional area of header M (nF_c/F_t) can be adjusted to improve flow distribution and pressure drop. An appreciate selection of these parameters do improve greatly uniformity of flow distribution. Thus, the straight parallel configurations should be selected since they have lowest pressure drops and low cost if a uniform flow distribution can be achieved after adjustment of parameters.

In spite of complexity and difficulty, the generalised theory formulated in this paper has linked performance, structural parameters and flow field configuration and is of significance to PEM fuel cell community. The present results demonstrated theoretically why non-uniform flow distributions occur and what key factors to control these phenomena. Particularly, it established a direct, systematic and quantitative relationship among structure, configuration and performance. This provides practical guideline how to improve flow fields and to design the fuel cell operating on an appropriate pressure and flow rate. The procedure of the design calculation is straightforward, in reality; no any iterative calculation is required due to fully explicit analytical solutions. Therefore, this work provides a flexible and direct tool for the designers of Z-type fuel cell layers and stacks.

CONCLUSIONS

BPs are a key component in fuel cells, which supply fuel and oxidant to reactive sites, remove water and heat, collect current and provide support for the cells in the stack. BPs typically account for 60~85% of the weight and 20~60% of the total cost in a fuel cell stack. It is well-known that performance of a fuel cell is stable in relatively narrow window operational conditions of electrochemistry. A small non-uniformity of flow distribution may lead significant deviation of some channels from the narrow window. Thus, non-uniform flow distribution leads non-uniform electrochemical reactions and causes critical issues of water, thermal and current management. Flow field designs in bipolar plates (BPs) are central to ensure uniform flow distribution and low pressure drop and to tackle systematically these critical issues. In spite of all the industrial R & D efforts, the gas flow fields in BPs remain one of the most important issues for high efficiency and cost reduction. In this paper, we will extend the generalised theoretical models of Z-type arrangement developed by Wang[18] from the parallel straight channels to other most common layout configurations, including single serpentine, multiple serpentine, and interdigitated layouts using the physical parameters of the structures: ratio of length to diameter and ratio of all the channel areas to head area for determining the performances of different layout configurations. The present generalised theory is the most generalised and completed and has unique capacities to compare directly, systematically and quantitatively different configurations, existing models and methodologies. The theory explained performances of different layout configurations and provided practical measures and guideline how to improve them.

In spite of complexity and difficulty, the rational yet tractable generalised model provides practical guideline how to improve flow fields and can contribute to the shared goal of cutting the currently high cost of new design and development of PEM fuel cells, which is central to a fuel cell engineer's "toolbox". Perhaps most importantly, it is a step forward to establish a direct, systematic and quantitative theoretical framework for different layout configurations in flow field designs in BPs. This has pointed the way toward a systematic assessment of configurations, structures and performances and interactions between them, which proves helpful in future flow field designs of fuel cells, and will stimulate further activity along this promising path. In this regard, a fruitful unified perspective is now emerging—one quite natural to fuel cell engineers. The results can also be used for the design guidance of flow distribution and pressure drop in other manifold systems and fuel cells, such as plate heat exchanges, plate solar collectors, distributors of fluidised bed and boiler headers and will stimulate further activity along this promising path.

REFERENCES

[1] Jeong, K.S., & Oh, B.S. (2002). Fuel Economy and Life-Cycle Cost Analysis of a Fuel Cell Hybrid Vehicle. *J Power Sources, 105*, 58-61.

[2] Li, X.G., & Sabir, I. (2005). Review of Bipolar Plates in PEM Fuel Cells: Flow-Field Designs. *Int J Hydrogen Energy, 30*, 359 – 371.

[3] De las Heras, N., Roberts E.P.L., Langton, R., & Hodgson, D.R. (2009). A review of metal separator plate materials suitable for automotive PEM fuel cells. *Energy Environ. Sci., 2*, 206–214.

[4] Hamilton, P.J., & Pollet, B.G. (2010). Polymer Electrolyte Membrane Fuel Cell (PEMFC) Flow Field Plate: Design, Materials and Characterisation. *Fuel Cells, 10*(4), 489–509.

[5] Anderson, R., Zhang, L., Ding, Y., Blanco, M., Bi, X., & Wilkinson, D. P. (2010). A Critical Review of Two-Phase Flow in Gas Flow Channels of Proton Exchange Membrane Fuel Cells. *Journal of Power Sources, 195*(15), 4531-4553.

[6] Barbir F., Gorgun, H., & Wang, X. (2005). Relationship Between Pressure Drop and Cell Resistance as a Diagnostic Tool for PEM Fuel Cells. *Journal of Power Sources, 141*, 96–101.

[7] Kumbur, E.C., Sharp, K.V., & Mench, M.M. (2006). Liquid Droplet Behavior and Instability in a Polymer Electrolyte Fuel Cell Flow Channel. *Journal of Power Sources, 161*, 333–345.

[8] Reiser, CA. (1989). Water and Heat Management in Solid Polymer Fuel Cell Stack. US Patent No. 4826742.

[9] Hsieh, S.S., Huang, Y.J., & Her, B.S. (2009). Pressure Drop on Water Accumulation Distribution for a Micro PEM Fuel Cell with Different Flow Field Plates. *International Journal of Heat and Mass Transfer, 52*, 5657–5659.

[10] Fletcher, N.J., Chow, C.Y., Pow, E.G., Wozniczka, B., Voss, H.H., Hornburg, G., & Wilkinson, D.P. (1995). Electrochemical Fuel Cell Stack with Concurrently Flowing Coolant and Oxidant Streams. Canadian Patent No. 2192170.

[11] Cavalca, C., Homeyer, S.T., & Walsworth, E. (1997). Flow Field Plate for Use in a Proton Exchange Membrane Fuel Cell. US Patent No. 5686199.

[12] Watkins, D.S., Dircks, K.W., & Epp, D.G. (1992). Fuel Cell Fluid Flow Field Plate. US Patent No. 5,108,849.

[13] Faghri, A., & Guo, Z. (2005). Challenges and Opportunities of Thermal Management Issues Related to Fuel Cell Technology and Modelling. *Int J Heat and Mass Transfer, 48*(19-20), 3891-3920.

[14] Lobato, J., Canizares, P., Rodrigo, M.A., Pinar, F.J., Mena, E., Ubeda, D. (2010). Three-Dimensional Model of a 50 cm2 High Temperature PEM Fuel Cell. Study of the Flow Channel Geometry Influence. *Int J Hydrogen Energy, 35*, 5510 – 5520.

[15] Chen, C.H., Jung, S.P., & Yen, S.C. (2007). Flow Distribution in the Manifold of PEM Fuel Cell Stack. *Journal of Power Sources, 173*, 249–263.

[16] Nie, J., & Chen, Y. (2010). Numerical Modeling of Three-Dimensional Two-Phase Gas–Liquid Flow in the Flow Field Plate of a PEM Electrolysis Cell. *Int J Hydrogen Energy, 35*, 3183 – 3197.

[17] Wang, J.Y. (2008). Pressure Drop and Flow Distribution in Parallel-Channel of Configurations of Fuel Cell Stacks: U-Type Arrangement. *Int. J. of Hydrogen Energy, 33*(21), 6339-6350.

[18] Wang, J.Y. (2010). Pressure Drop and Flow Distribution in Parallel-Channel of Configurations of Fuel Cell Stacks: Z-Type Arrangement. *Int. J. of Hydrogen Energy, 35*, 5498-550.

[19] Wang, J.Y., & Wang, H.L. Flow Field Designs of Bipolar Plates in PEM Fuel Cells: Theory and Applications.

[20] Bajura, RA. (1971). A Model for Flow Distribution in Manifolds. *J. Engineering for Power, Transaction of ASME, 93*, 7-12.

[21] Bajura R.A., & Jones Jr. E.H. (1976). Flow Distribution Manifolds. *J. Fluid Eng., Transaction of ASME, 98*, 654–65.

[22] Bassiouny, M.K., & Martin, H. (1984). Flow Distribution and Pressure Drop in Plate Heat Exchanges. Part II. Z-Type Arrangement. *Chem. Eng. Sci., 39*(4), 7001–704.

[23] Kee, R.J., Korada, P., Walters, K., & Pavol, M. (2002). A Generalized Model of the Flow Distribution in Channel Networks of Planar Fuel Cells. *J Power Sources; 109*, 148-159.

[24] Maharudrayya, S., Jayanti, S., & Deshpande, A.P. (2005). Flow Distribution and Pressure Drop in Parallel-Channel Configurations of Planar Fuel Cells. *J Power Sources, 144*, 94-106.

[25] Chang, P.A.C., St-Pierre, J., Stumper, J., & Wetton B. (2006). Flow Distribution in Proton Exchange Membrane Fuel Cell Stacks. *J Power Sources, 162*, 340-355.

[26] Koh, J.H., Seo, H.K., Lee, C.G., Yoo, Y.S., & Lim, H.C. (2003). Pressure and Flow Distribution in Internal Gas Manifolds of a Fuel Cell Stack. *J Power Sources, 115*, 54-65.

[27] Yao, K.Z., Karan, K., McAuley, K.B., Oosthuizen, P., Peppley, B., Xie, T. (2004). A Review of Mathematical Models for Hydrogen and Direct Methanol Polymer Electrolyte Membrane Fuel Cells. *Fuel Cells, 4*(1-2), 3-29.

[28] Wang, J.Y. (2011). Theory of Flow Distribution in Manifolds. *Chemical Engineering J, 168*, 1331-1345.

[29] Pigford, R.L., & Miron, A.M. (1983). Flow Distribution in Piping Manifolds. *Ind. Eng. Chem. Fundam., 22*, 463-471.

[30] Wang, J.Y. (2009). Comments on "Flow Distribution in U-Type Layers or Stacks of Planar Fuel Cells", by W.H. Huang and Q.S. Zhu [J. of Power Sources, 178, 353-362]. *J. of Power Sources, 190*(2), 511-512.

